

Feasibility Study of Pion and Kaon Structure via the Sullivan Process at EicC

Zongyang Lu^a, Zihan Yu^a, Ting Lin^a, Yu-Tie Liang^{b,c},

Rong Wang^{b,c}, Wan Chang^d, and Weizhi Xiong^a

^a*Key Laboratory of Particle Physics and Particle Irradiation (MOE),*

Institute of Frontier and Interdisciplinary Science,

Shandong University, Qingdao, Shandong 266237, China

^b*Institute of Modern Physics, Chinese Academy of Sciences, Lanzhou 730000, China*

^c*University of Chinese Academy of Sciences, Beijing 100049, China and*

^d*School of Physics and Electronic Engineering,*

Nanyang Normal University, Nanyang 473061, China

Abstract

The Electron–Ion Collider in China (EicC) provides an excellent opportunity to explore the internal structure of pions and kaons via the Sullivan process in deep-inelastic scattering (DIS). In this study, we present detailed projections for the pion and kaon structure functions, F_2^π and F_2^K , at EicC, with a focus on both statistical and systematic uncertainties. Leveraging EicC’s high luminosity and broad kinematic coverage, the accessible kinematic region is extended beyond previous measurements. The projected statistical uncertainties for F_2^π and F_2^K are below 5% and 8%, respectively, across most kinematic bins. Systematic uncertainties arising from detector effects have been carefully evaluated. These results significantly enhance the precision of meson structure function measurements and provide important constraints on theoretical models of meson parton distributions. Moreover, this study bridges the gap between fixed-target and collider-era measurements, highlighting the pivotal role of EicC in advancing our understanding of hadronic structure.

I. INTRODUCTION

The pion is the lightest meson, while the kaon is the lightest meson containing a strange quark in the Standard Model, with each composed of a quark–antiquark pair bound by the strong interaction. Their simplicity makes them ideal probes of Quantum Chromodynamics (QCD), the theory describing the strong force. Pions are nearly ideal realizations of pseudo-Nambu–Goldstone bosons [1, 2], arising from the spontaneous breaking of chiral symmetry in QCD, while kaons provide an essential window into the interplay between light and strange quarks. Together, they form a unique platform for exploring the low-energy domain of QCD, where perturbative methods break down and nonperturbative dynamics dominate [3–6].

Recent progress in lattice QCD [7–11], Dyson–Schwinger method [12–16], and effective field theories [17–19], together with high-energy scattering experiments [20–34], has enabled increasingly precise investigations of pion and kaon structure. These studies have advanced our knowledge of their electromagnetic form factors, parton distribution functions (PDFs), and generalized parton distributions (GPDs). Data from facilities such as Jefferson Lab [35–39], HERA [40] experiments including H1 [41] and ZEUS [42], CERN fixed-target experiments [43, 44], and the future Electron–Ion Collider (EIC) [45–47], combined with theoretical developments, have revealed that mesons are far from pointlike: their internal structure is significantly more intricate than suggested by constituent-quark models [6, 48]. Despite these advances, a comprehensive understanding of their partonic structure remains incomplete.

A powerful method to access the structure of these unstable mesons is the Sullivan process [8, 9, 49, 50], in which deep-inelastic scattering off the virtual meson cloud of a nucleon, effectively providing a pion or kaon target. This approach overcomes the limitation of mesons’ short lifetimes and has been validated in previous experiments for pions [41, 42, 51]. For kaons, the method presents additional challenges due to the suppressed strange-quark component in the nucleon’s meson cloud, but it remains a viable strategy for extracting their partonic structure [6].

The EicC [52] offers a unique opportunity to probe the internal structure of hadrons with particular emphasis on the sea-quark region. In this work, we develop a production model

based on the Sullivan process to investigate the structure of pions and kaons. By examining the relevant kinematics and detector requirements, we present detailed projection studies of their structure function at EicC. The remainder of this paper is organized as follows: Section 2 outlines the theoretical framework and the implementation of the Sullivan process in our analysis. Section 3 describes the conceptual design of the experimental setup and the strategies for event selection and analysis. Section 4 presents the main results, including comparisons with theoretical predictions and existing data. Finally, Section 5 summarizes the key findings and discusses prospects for future research.

II. KINEMATICS AND CROSS SECTION

Figure 1 shows the Feynman diagrams for semi-inclusive leading neutron (a) and Λ (b) production in collisions via the Sullivan process. In this framework, the process $ep \rightarrow eX\mathcal{B}$, where \mathcal{B} represents the leading baryon, provides access to the structure of unstable mesons. The process is fully described by four kinematic variables:

$$Q^2 = -q^2 = -(k - k')^2, \quad x_B = \frac{Q^2}{2P \cdot q},$$

$$y = \frac{q \cdot P}{k \cdot P} \simeq \frac{Q^2}{sx_B}, \quad W^2 = (P + k - k')^2 = m_p^2 + \frac{Q^2(1 - x_B)}{x_B}, \quad (1)$$

where k , P , k' , and N represent the four-momenta of the incoming electron (e), proton (p), scattered electron (e'), and leading baryon (n or Λ), respectively, and m_p is the proton mass. When probing the pion structure, the final-state baryon is a neutron ($\mathcal{B} = n$); for the kaon structure, it is a Λ ($\mathcal{B} = \Lambda$). In this process, the energy fraction of the final-state hadron x_L , and the squared four-momentum transfer of the target proton t , are expressed as:

$$x_L = \frac{N \cdot k}{P \cdot k}, \quad t = (P - N)^2 \quad (2)$$

respectively. The exchanged virtual pion or kaon can then be treated as an effective target. Analogous to the Bjorken variable, the momentum fraction of the struck constituent inside the meson is defined as:

$$x_{\mathcal{M}} = \frac{Q^2}{2P_{\mathcal{M}} \cdot q} = \frac{x_B}{1 - x_L} \quad (3)$$

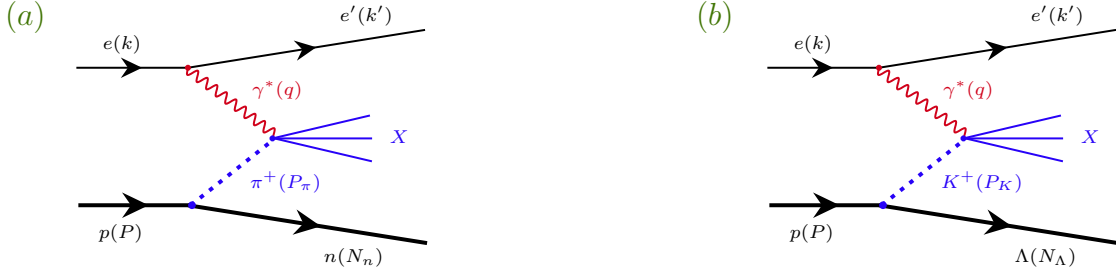


FIG. 1. Sullivan process in DIS. (a) Pion case: the proton emits a virtual π^+ and transitions into a neutron. (b) Kaon case: the proton emits a virtual K^+ and transitions into a Λ .

Thus, the differential cross section for leading neutron or Λ production in the process $ep \rightarrow e'X\mathcal{B}$ can be written as [41, 42, 53]

$$\begin{aligned} \frac{d^4(\sigma \rightarrow eX\mathcal{B})}{dx_B dQ^2 dx_L dt} &= \frac{4\pi\alpha^2}{x_B Q^4} \left(1 - y + \frac{y^2}{2}\right) F_2^{LB(4)}(Q^2, x_B, x_L, t) \\ &= \frac{4\pi\alpha^2}{x_B Q^4} \left(1 - y + \frac{y^2}{2}\right) F_2^{\mathcal{M}}\left(\frac{x_B}{1-x_L}, Q^2\right) f_{\mathcal{M}/p}(x_L, t), \end{aligned} \quad (4)$$

where $\mathcal{M} = \pi^+$ or K^+ , and $F_2^{LB(4)}(Q^2, x_B, x_L, t)$ denotes the semi-inclusive structure function. In this expression, the leading-baryon structure function $F_2^{LB(4)}$ factorizes into the meson structure function $F_2^{\mathcal{M}}$ and the meson flux surrounding the proton, $f_{\mathcal{M}/p}$.

In the effective field theory, the meson flux is typically evaluated at the pion or kaon pole [54–61],

$$f_{\mathcal{M}/p}(x_L, t) = \frac{1}{2\pi} \frac{g^2}{4\pi} (1 - x_L) \frac{-t}{(m_{\mathcal{M}}^2 - t)^2} \exp\left(\mathcal{C} R_{\mathcal{B}\mathcal{M}}^2 \frac{t - m_{\mathcal{M}}^2}{1 - x_L}\right), \quad (5)$$

where $m_{\mathcal{M}}$ is the meson mass. For pions and kaons, the relevant coupling constants are $g = g_{pn\pi}$ and $g = g_{N\Lambda K}$, with $g_{pn\pi}^2/4\pi = 13.6$ [62] and $g_{N\Lambda K}^2/4\pi = 14.7$ [56], respectively. The interaction radii are $R_{n\pi} = 0.93 \text{ GeV}^{-1}$ [60] for the $n - \pi$ system and $R_{\Lambda K} = 1.0 \text{ GeV}^{-1}$ [56] for the $\Lambda - K$ system. The parameter \mathcal{C} is an auxiliary sign factor introduced to unify the expression: $\mathcal{C} = 1$ for the $n - \pi$ system and $\mathcal{C} = -1$ for the $\Lambda - K$ system.

III. EICC DETECTOR

EicC is a proposed high-energy nuclear physics facility designed to probe the internal structure of hadrons, with particular emphasis on the sea-quark region, as well as to investigate exotic hadronic states and the properties of nuclear matter [52, 63, 64]. With a

tunable center-of-mass energy of 15–20 GeV and a luminosity exceeding $10^{33} \text{ cm}^{-2}\text{s}^{-1}$, EicC will enable unprecedented precision in measurements of sea-quark dynamics. The collider is designed to operate by default with a 3.5 GeV electron beam and a 20 GeV proton beam, achieving a luminosity nearly two orders of magnitude higher than that of the former HERA [40] collider in Germany, thereby providing a wealth of high-precision data on hadron structure. A central detector and a set of forward detectors constitute key components of the EicC experimental setup. The central detector provides large acceptance, with a pseudorapidity coverage from $\eta = -3.5$ to 3.5 , enabling comprehensive tracking and particle identification over a wide kinematic region. The forward detectors are optimized for detecting leading baryons and mesons produced at high pseudorapidity, particularly from beam remnants and diffractive processes. Complementary to the U.S. Electron–Ion Collider, which focuses on the gluon-dominated regime at higher energies, EicC will play a crucial role in advancing the next era of precision nuclear physics research.

To assess the feasibility of measuring the pion and kaon structure functions at the EicC via the Sullivan process, we performed dedicated Monte Carlo simulations focusing on channels involving pion and kaon structure. The detector response was modeled using the EicC fast simulation framework [65–67]. Event generation was carried out with the **Tagged-neutron-DIS** [58, 68] and **Tagged-Lambda-DIS** [56, 69] generators, both implemented in C++ and based on the CERN ROOT framework [70]. For the LN-DIS process, the generator incorporates comparisons among the global JAM18 fit [71], available experimental data, and predictions from the dynamical parton model. In particular, the pion PDFs were taken from the **piIM-Parton** set [72, 73], derived within the dynamical parton distribution framework. For the LA-DIS process, where information on the kaon structure is highly limited and only a few global kaon PDF analyses exist [74–77], the generator employs a kaon PDF obtained from a model-dependent analysis constrained solely by the NA3 data [78], also within the dynamical parton model framework.

Figure 2 illustrates the event distributions of the generated LN-DIS process within the selected kinematic region. As shown in the left panel, the events populate a broad kinematic phase space, with a higher density observed at relatively small Q^2 and x_B , where the virtual photon predominantly probes low-momentum partons in the meson cloud. Under the applied selection cuts, x_B extends up to approximately 0.25. In contrast, the right panel displays the event distribution in the (x_π, t) plane, covering almost the entire accessible kinematic range.

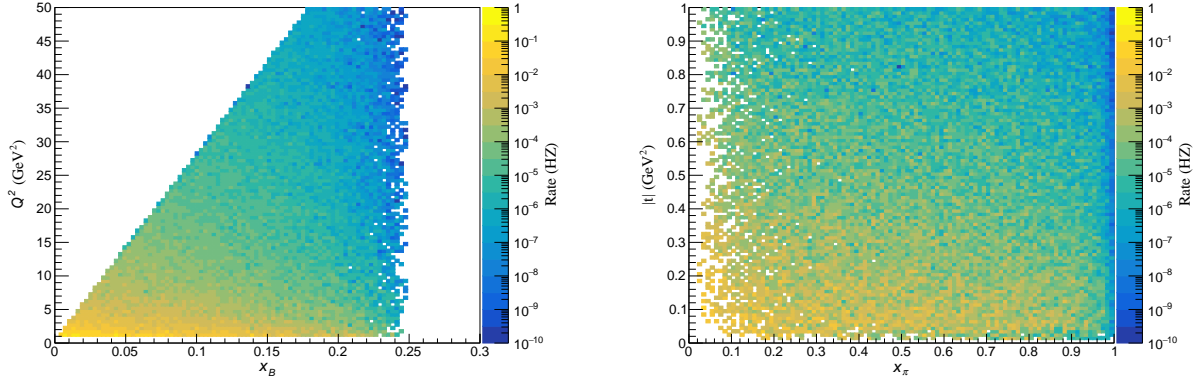


FIG. 2. Event rates for the LN-DIS process at the EicC, obtained from Monte Carlo simulation and shown as two-dimensional histograms of invariant kinematic variables. Left panel: distribution in (x_B, Q^2) . Right panel: distribution in $(x_\pi, |t|)$. The MC events were generated within the kinematic region $0.01 \text{ GeV}^2 < |t| < 1 \text{ GeV}^2$, $0.75 < x_L < 1$, $x_B < 1$, $1 \text{ GeV}^2 < Q^2 < 50 \text{ GeV}^2$, and $W^2 > 4 \text{ GeV}^2$.

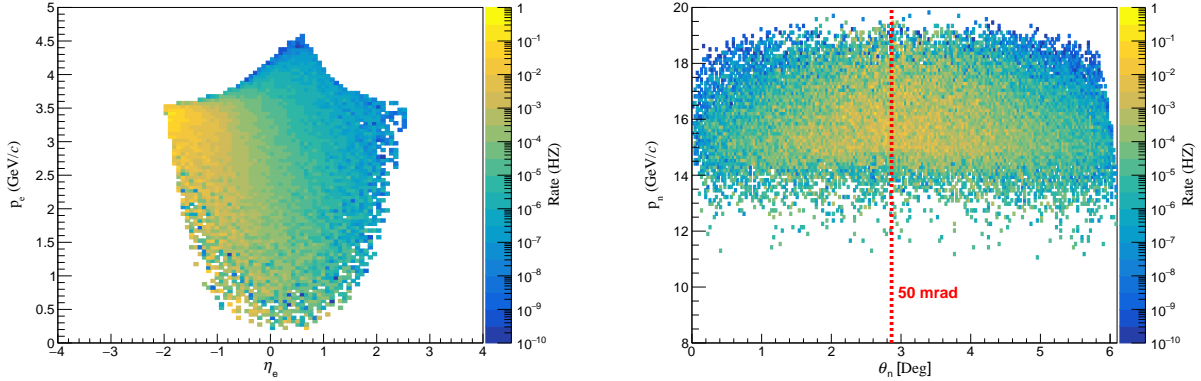


FIG. 3. For the Sullivan process $ep \rightarrow enX$, the left panel shows the correlation between the scattered electron momentum and pseudorapidity η , while the right panel depicts the relationship between the detected neutron momentum and scattering (polar) angle. The distributions are approximately symmetric with respect to the incident proton beam, which is designed to have a crossing angle of 50 mrad (about 2.86°). All cases correspond to the energy setting of a 3.5 GeV electron colliding with a 20 GeV proton. The distributions for the $ep \rightarrow e\Lambda X$ process exhibit a similar pattern.

A clear correlation is visible, with the event density gradually decreasing from the small- x_π , small- $|t|$ region toward the large- x_π , large- $|t|$ region. This behavior reflects the characteristic t -dependence of the meson-exchange mechanism inherent to the Sullivan process. Over-

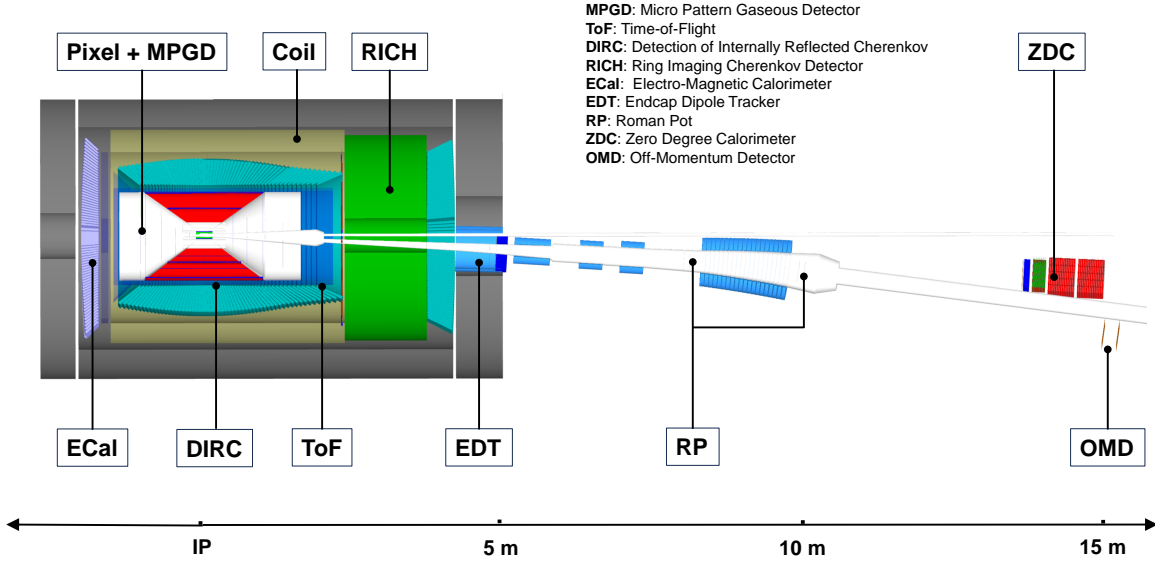


FIG. 4. Conceptual design of the EicC detector, with the central and ion far-forward detectors included.

all, these distributions confirm the expected kinematic features of meson-exchange-induced DIS and demonstrate the feasibility of probing meson structure via leading-baryon tagged measurements at the EicC. In the LN-DIS process, the scattered electron and the produced hadronic system originate from a hard interaction between the virtual photon and the meson cloud surrounding the proton. As shown in Figure 3, the scattered electrons are primarily distributed within the central rapidity region ($|\eta| < 3.5$) with a broad momentum range, where the central detector of the EicC provides precise tracking and particle identification with an efficiency exceeding 95%. In contrast, the final-state neutron emerges at a very small angle relative to the incident proton beam, typically within a few tens of milliradians, while carrying a large fraction of the proton's initial momentum. This kinematic feature underscores the need for a dedicated far forward detection system.

As illustrated in Fig. 4, the EicC far-forward detector system consists of several sub-detectors, including the Endcap Dipole Tracker (EDT), Roman Pots (RP), Off-Momentum Detector (OMD), and the Zero Degree Calorimeter (ZDC). These detectors operate collaboratively to reconstruct neutrons, photons, and charged hadrons produced at extremely small scattering angles.

The ZDC detects neutrons within approximately 15 mrad of the ion-beam direction and

provides sufficient performance for reconstructing the four-momentum transfer t . According to simulation studies, the ZDC achieves an energy resolution of

$$\frac{\sigma_E}{E} \approx \frac{48.7\%}{\sqrt{E [\text{GeV}]} + 1.9\%}, \quad (6)$$

and a transverse position resolution of

$$\sigma_x \approx \frac{3 \text{ cm}}{\sqrt{E [\text{GeV}]}} \quad (7)$$

corresponding to an angular resolution of approximately $2.1 \text{ mrad}/\sqrt{E [\text{GeV}]}$ at a distance of 14 m from the IP. This performance enables a typical t resolution of about 0.03 GeV^2 .

The EDT, RP, and OMD jointly reconstruct the charged decay products of the Λ baryon produced in the Λ -DIS process. The Λ decays predominantly via the charged channel ($\Lambda \rightarrow p\pi^-$, BR $\sim 64\%$) and the neutral channel ($\Lambda \rightarrow n\pi^0 \rightarrow n\gamma\gamma$, BR $\sim 36\%$). Reconstructing this topology requires the combined acceptance of all forward detectors.

For charged decay channel, the proton is reconstructed using the combined tracking information from the EDT, RP, and OMD. The EDT provides tracking in $15 \text{ mrad} < \theta < 60 \text{ mrad}$ with a momentum resolution of

$$\frac{\sigma_p}{p} \approx 0.6\%, \quad (8)$$

and a polar-angle resolution better than 3 mrad. The RP extends charged-particle tracking down to 5 mrad and achieves an improved momentum resolution of

$$\frac{\sigma_p}{p} \approx 0.2\%. \quad (9)$$

The OMD captures low-momentum decay protons with $0.4 < x_L < 0.75$, requiring a spatial resolution of order $100 \mu\text{m}$, achievable with Monolithic Active Pixel Sensors (MAPS) or Micro-Pattern Gaseous Detectors (MPGDs). The π^- from the decay is accepted and reconstructed solely by the EDT tracking system.

For neutral decay channel, the neutron is tagged by the ZDC, while the two photons from the π^0 decay are jointly reconstructed using the ZDC, the EDT electromagnetic calorimeter (EDT-ECal), and the hadron-endcap ECal of the central detector.

The capability of reconstructing Λ baryons over a wide kinematic range is particularly relevant for studies of the kaon structure via the Sullivan process. In such measurements,

the final-state Λ carries critical information about the kaon, and efficient reconstruction of its decay products directly impacts the precision and reach of the structure-function extraction. Therefore, the performance of the far-forward detector system—both in charged and neutral decay channels—is a key factor in determining the sensitivity of kaon-structure measurements.

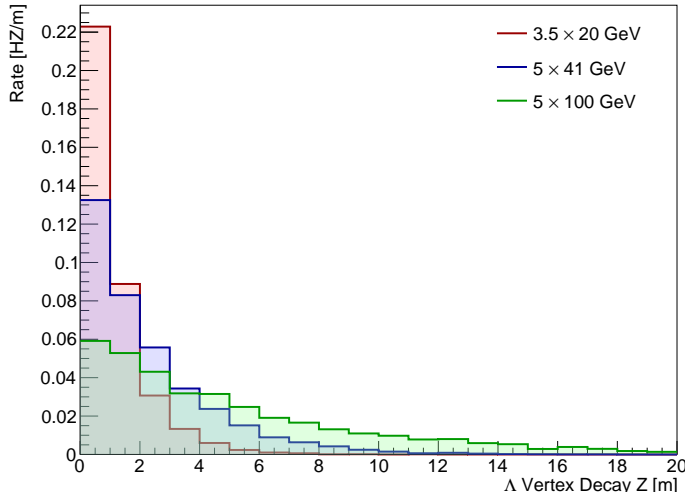


FIG. 5. Distribution of the Λ decay vertex along the z direction for final-state Λ at different collision energies.

With this capability in place, the EicC offers unique advantages for studying the kaon structure. Since the kaon structure is accessed via the Sullivan process, the reconstruction of the Λ baryon in the final state is essential. The Λ has a relatively long lifetime of $\tau = (2.617 \pm 0.010) \times 10^{-10}$ s [79], meaning that at high beam energies its decay length can easily exceed several tens of meters. Figure 5 shows the distribution of the Λ decay vertex along the flight direction at different collision energies. For the typical EicC configuration of 3.5×20 GeV, more than 95% of Λ baryons decay within 5 m of the interaction point—well within the coverage of the forward detector system. In contrast, for the lower-energy EIC configuration of 5×41 GeV, only about 80% of Λ baryons decay within 5 m, and this fraction drops below 60% for higher energies such as 5×100 GeV. Consequently, under comparable luminosity conditions, the EicC detector is expected to have a higher detection efficiency for kaon-structure measurements. Moreover, the larger crossing angle allows for a more spacious detector design, which further enhances the overall detection efficiency.

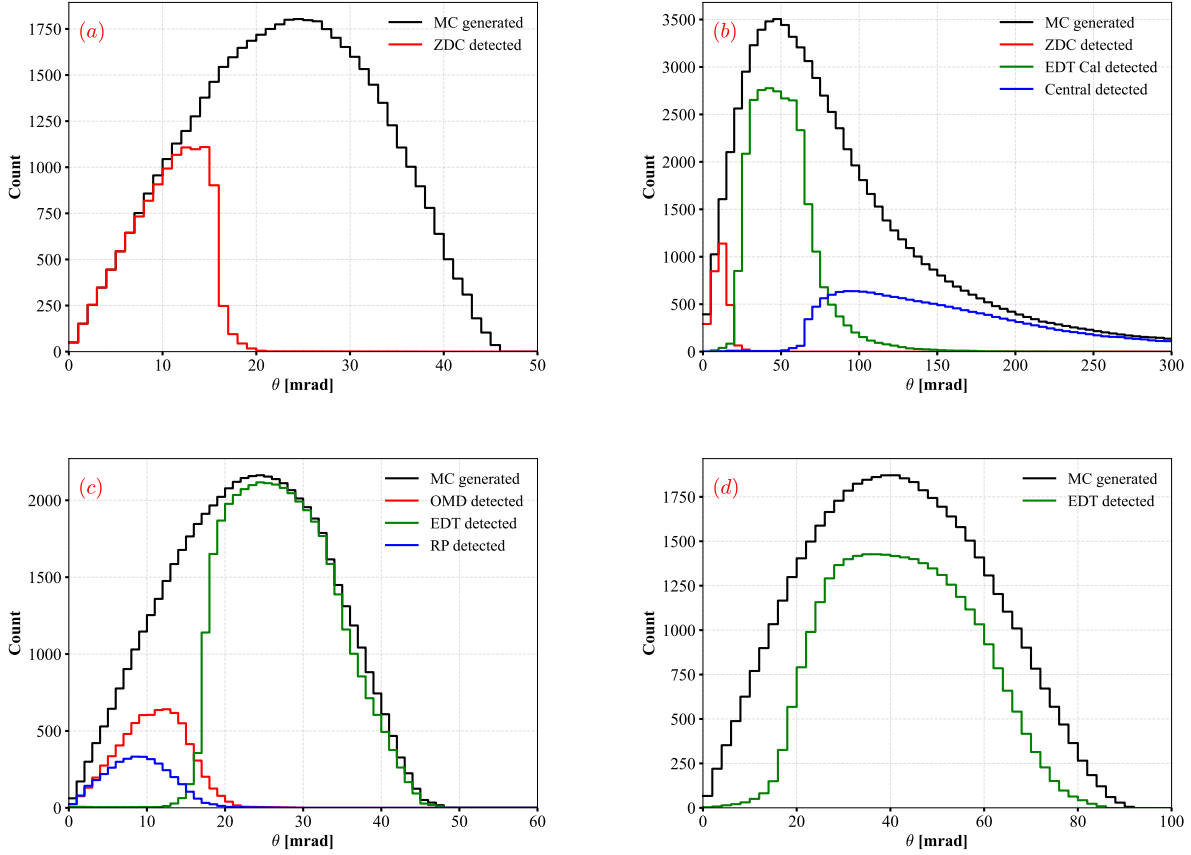


FIG. 6. Angular distributions and detector acceptances for neutrons (a) and photons (b) from the neutral Λ decay mode, and for decay protons (c) and π^- mesons (d) from the charged Λ decay mode, for a 20 GeV proton beam on a 3.5 GeV electron beam.

Building on these kinematic and detector advantages, the reconstruction performance of Λ decays at EicC is illustrated in Figure 6, which shows the angular distributions of the Λ decay products—(a) neutron and (b) photon from the neutral decay channel, and (c) proton and (d) π^- from the charged decay channel—together with their corresponding acceptance in the far forward detector system. Building upon these reconstruction capabilities, the kaon structure function can be measured following a strategy analogous to that used for the pion. By focusing on the charged decay channel, which dominates the statistics and offers higher detection efficiency, the impact of detector-resolution effects is mitigated compared with the pion measurement, as both the final-state proton and pion can be reconstructed with high precision. Overall, the full far-forward detector system yields an approximate Λ detection efficiency of about 40%, with the charged decay channel contributing roughly 55% and the

neutral channel about 15%.

IV. STRUCTURE FUNCTION

To reliably extract the meson structure functions via the Sullivan process, it is essential to isolate events of interest with high purity. Figure 7 illustrates the key kinematic distributions used to separate Sullivan events from generic DIS backgrounds, with the DIS sample generated using the `PYTHIA 8` event generator [80]. As shown in Fig. 7(a), after applying the kinematic requirements $x_L > 0.75$, $M_X > 0.5$ GeV, and $W^2 > 4$ GeV², the pseudorapidity distribution of the final-state neutron exhibits a pronounced peak in the far-forward region, showing a clear dominance of events at $\eta_n > 4$, which enables efficient background suppression. The ZDC covers the region $\eta_n > 5$, which naturally helps to suppress background. Figure 7(b) shows the x_L distributions of DIS and Sullivan events after applying the cuts $\eta_n > 5$, $p_T^n < 0.3$ GeV, $M_X > 0.5$ GeV, and $W^2 > 4$ GeV². The x_L variable is a powerful discriminator for the two different processes, with the Sullivan events peak strongly at large x_L , whereas DIS backgrounds fall off at high x_L . A final requirement of $x_L > 0.75$ and $\eta_n > 5$, indicated by the vertical dashed lines, yields a Sullivan-event purity exceeding 90%. In addition, conventional cuts of $0.01 < |t| < 1$ GeV² and $x_B < 1$ were applied to ensure that the simulated data follow physically realistic distributions.

The extraction of the meson structure functions is performed in bins of $(x_{\mathcal{M}}, Q^2)$. The event generator provides, for each generated event, the differential cross section and the corresponding event rate. When filling the histograms, each event is weighted by the product of its rate and the assumed integrated luminosity, such that the resulting distributions represent the expected yield under realistic running conditions.

For each $(x_{\mathcal{M}}, Q^2)$ bin, the differential yield as a function of the squared momentum transfer t of the forward baryon is constructed. The relation between the four-fold differential cross section and the meson structure function is given by Eq. 4, which factorizes the measured cross section into the structure function $F_2^{\mathcal{M}}$ and the meson flux factor $f_{\mathcal{M}/p}(x_L, t)$. In the extraction, the flux $f_{\mathcal{M}/p}(x_L, t)$ is fixed using a chosen flux model, while $F_2^{\mathcal{M}}$ is determined by fitting the t distribution with Eq. 4. The statistical uncertainty of $F_2^{\mathcal{M}}$ is taken from the covariance matrix of the fit.

The systematic uncertainty assessment has been performed with particular emphasis on

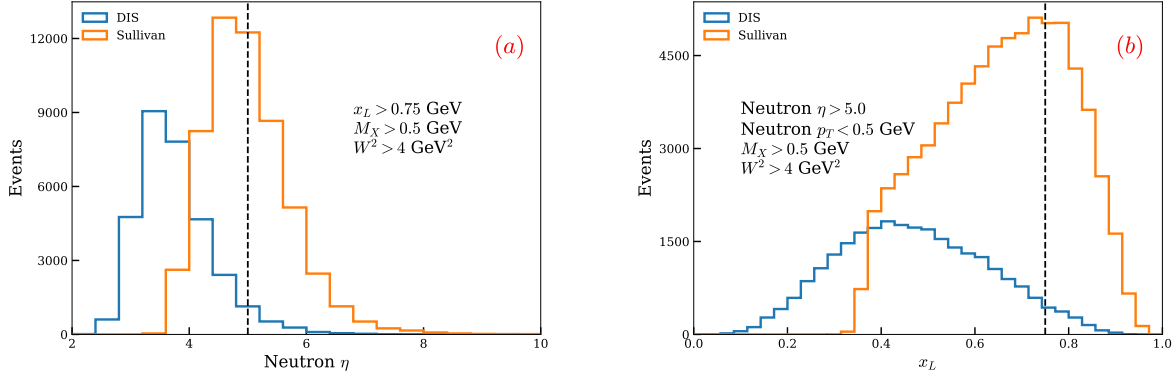


FIG. 7. Kinematic distributions of the final-state neutron in DIS (blue) and Sullivan (orange) events. (a): Pseudorapidity (η) distribution of the neutron after applying $x_L > 0.75$, $M_X > 0.5$ GeV, and $W^2 > 4$ GeV². The dashed line at $\eta = 5$ indicates the selection cut used to achieve high Sullivan purity. (b): Distribution of x_L for the neutron after applying $\eta > 5$, $p_T < 0.3$ GeV, $M_X > 0.5$ GeV, and $W^2 > 4$ GeV². The dashed line at $x_L = 0.75$ indicates the final selection threshold used to achieve high Sullivan purity.

detector-related effects. These studies were first carried out for the pion measurement, followed by a parallel evaluation for the kaon measurement.

The important source of systematic uncertainty arises from detector resolution effects. These were implemented by applying Gaussian smearing to the true four-momentum vectors of both the scattered electron and the forward neutron. For the scattered electron, the momentum, polar angle, and azimuthal angle were independently smeared according to the parameterized resolutions obtained from the EicC fast simulation. For the forward neutron detected in the ZDC, the energy and impact position on the detector plane were smeared using the energy-dependent resolutions given by the position resolution in Eq. 7 and the energy resolution in Eq. 6. The resulting smeared four-momentum vectors were propagated through the reconstruction chain to incorporate realistic detector effects.

To estimate the uncertainty associated with these resolutions, the energy and position smearing parameters were varied by $\pm 10\%$, and the induced variations in the reconstructed distributions were taken as the corresponding systematic uncertainty. As an additional cross-check, both smeared and unsmeared distributions were fitted using Eq. 4. The detector-resolution uncertainty contributes approximately 10% to the pion measurement.

Beyond detector resolution, several additional sources of systematic uncertainty were

evaluated. A 3% uncertainty arises from luminosity normalization, reflecting the precision of the integrated luminosity determination. Acceptance corrections introduce another 8% uncertainty due to potential mismodeling of the detector acceptance across the relevant kinematic range. The ratio method [42], which extracts the pion structure function by taking the ratio of tagged to inclusive DIS yields to cancel common systematic effects, introduces an additional 2% uncertainty associated with the proton structure function F_2^p . These contributions together form the complete systematic uncertainty budget for the pion measurement.

In the analysis of the kaon structure function, we use only the charged decay channel for now for simplicity. The associated systematic uncertainty study is performed following the same methodology as in the pion case. Detector-resolution effects were evaluated by applying the identical smearing procedure to the kaon sample. However, because the reconstructed final state predominantly comes from the decay $\Lambda \rightarrow p\pi^-$, whose charged decay products are efficiently measured by the tracking system, the overall momentum resolution is significantly improved. Consequently, the detector-resolution uncertainty for the kaon measurement is reduced to approximately 5%.

In addition, the background process $ep \rightarrow e'\Sigma^0 X$, $\Sigma^0 \rightarrow \Lambda\gamma$ introduces a non-negligible systematic uncertainty to the kaon structure-function measurement. Since both the signal process $ep \rightarrow e\Lambda X$ and the background channel produce a Λ baryon in the final state, the contamination from Σ^0 production must be taken into account. To estimate this effect, we compared the hadronic couplings $g_{K\Lambda N}$ and $g_{K\Sigma N}$ using values reported in various theoretical studies [81–93], which suggests that the relative size of the Σ^0 contribution could be at the level of approximately 10%. However, the charged decay mode $\Sigma^0 \rightarrow \Lambda\gamma$ can be partially vetoed when the decay photon from Σ^0 has sufficient energy. Taking this into consideration, we adopt a conservative estimate of a residual $\sim 5\%$ systematic uncertainty associated with the Σ^0 background.

All remaining sources of systematic uncertainty—including luminosity normalization, acceptance effects, and uncertainties from the ratio method—are treated using the same procedures as in the pion analysis, ensuring full consistency across both measurements.

Based on all the sources of uncertainty discussed above, Fig. 8 presents the systematic and statistical uncertainties for the pion (left panel) and kaon (right panel) structure-function extractions across the relevant kinematic ranges. For the pion measurement, the accessible

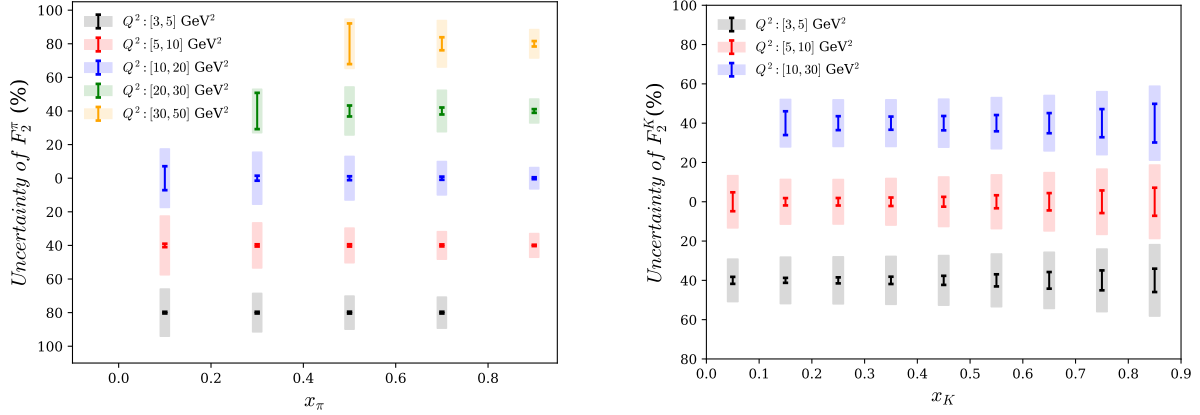


FIG. 8. **Left panel:** Projected pion structure function F_2^π at EicC, showing statistical uncertainties (error bars) and systematic uncertainties (color bands, excluding the flux factor) for different x_π and Q^2 bins. **Right panel:** Projected kaon structure function F_2^K at EicC, showing similar analysis results. Both cases assume an integrated luminosity of 50 fb^{-1} and an energy setting of $3.5 \times 20 \text{ GeV}^2$.

kinematics span $Q^2 = 3\text{--}50 \text{ GeV}^2$ and $x_\pi = 0\text{--}1$. For $Q^2 > 5 \text{ GeV}^2$, the statistical uncertainty in each analysis bin falls below 5%, reaching the precision necessary for detailed studies of the pion structure function. In this channel, the ZDC dominates the systematic uncertainty, with its energy and position resolutions discussed in Sec. III, and the reconstruction of the squared momentum transfer achieving a resolution of approximately $\Delta t \sim 0.03 \text{ GeV}^2$. For the kaon measurement (right panel), the analysis employs the charged decay channel $\Lambda \rightarrow p\pi^-$, achieving Q^2 coverage up to 30 GeV^2 . Thanks to the charged decay tracks, the momentum transfer t of the Λ can be reconstructed with a resolution of about $\Delta t \sim 0.0075 \text{ GeV}^2$, and the overall reconstruction efficiency of the charged decay exceeds 50%. The statistical uncertainty remains below 8% for all bins, enabling precise studies of the kaon structure function. Overall, these results demonstrate that EicC offers unique advantages for kaon structure-function measurements through the Sullivan process.

In Fig. 9, we present the projected measurements of the pion valence up-quark distribution, $x_\pi u_v^\pi(x_\pi)$, at the EicC for five representative Q^2 bins ranging from 3 to 50 GeV^2 . The total uncertainties, shown as error bars, include both statistical and estimated systematic contributions combined in quadrature. A comparison is made with existing Drell-Yan data [94], future JLab projections [95], and several theoretical predictions, including Dyson-Schwinger approaches [96, 97], perturbative QCD fits [71], and the GRV-P param-

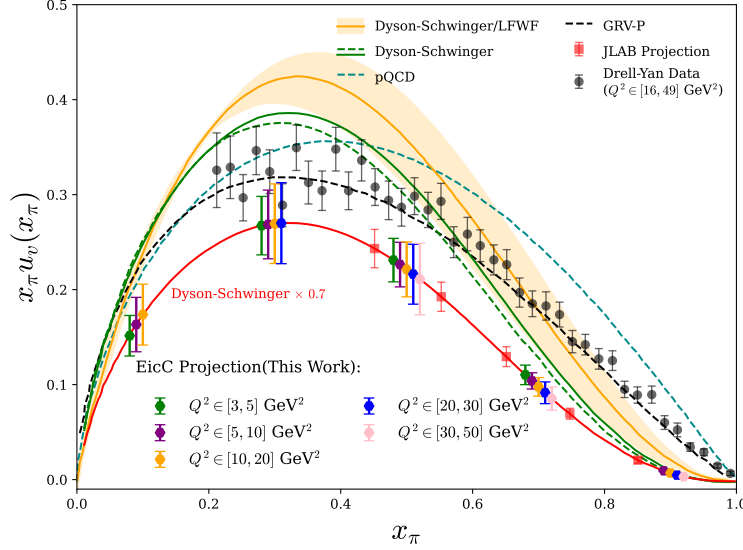


FIG. 9. Projected measurements of the pion valence up-quark distribution $x_\pi u_v^\pi(x_\pi)$ at the EicC in several Q^2 bins (colored points with error bars), compared with existing data from Drell-Yan experiments (black circles) [94], JLab projections (red squares) [95], and various theoretical predictions including Dyson-Schwinger (green and orange bands/curves) [96, 97], pQCD (teal dashed line) [71], and GRV-P (black dashed line) [96]. The red solid curve shows the Dyson-Schwinger prediction scaled by a factor of 0.7. The error bars on the EicC projections represent the combined statistical and estimated systematic uncertainties.

eterization [96]. The EicC provides unprecedented sensitivity to the intermediate-to-large x_π region in Sullivan-process measurements, a kinematic domain where no data from Sullivan experiments are currently available, thereby offering crucial new information on the pion's structure in the nonperturbative valence region. While the pion structure function has been constrained by previous measurements, experimental information on the kaon structure function remains very limited. Therefore, the kaon structure function measurements at the EicC will be particularly valuable.

With the projected precision demonstrated above, the EicC data can be meaningfully combined with existing and future Drell-Yan measurements. Compared with the existing world data, the EicC extends the accessible Q^2 coverage by a factor of 2–3 beyond JLab-12 GeV, effectively bridging the gap between fixed-target and collider-era measurements. Since the Drell-Yan process is independent of the meson flux, its extracted structure functions are free of flux-model uncertainties. Therefore, combining the Drell-Yan measurements

with the EicC Sullivan data in the overlapping kinematic region can substantially reduce the model-dependent systematic uncertainties, particularly those originating from the pion flux. In practice, the model uncertainty associated with the pion flux is typically estimated to be on the order of $\sim 10\text{--}25\%$ [41, 42, 46]. A combined analysis of the EicC measurements and pion Drell–Yan data in the same kinematic regime, such as those from AMBER and Fermilab [94, 98], is expected to significantly constrain and reduce this flux-related uncertainty.

V. SUMMARY AND OUTLOOK

This study investigates the feasibility and expected precision of measuring the meson structure functions F_2^π and F_2^K at the proposed EicC, based on the Sullivan process. By selecting final-state forward baryons based on their x_L distributions in the far forward region, high-purity Sullivan events can be identified, with the deep inelastic scattering background effectively suppressed. Within each (x_M, Q^2) bin, the meson structure functions are extracted by fitting the differential yields as a function of the baryon momentum transfer t . Detector resolution effects are simulated by applying Gaussian smearing to the four-momenta of the electron and forward baryon, while systematic uncertainties are evaluated through a combination of variations in resolution, acceptance corrections, and other methods. Under the nominal EicC running conditions with an integrated luminosity of 50 fb^{-1} , the statistical precision of F_2^π reaches better than 5% in the key kinematic region ($Q^2 > 5\text{ GeV}^2$), while the overall statistical uncertainty of F_2^K is controlled within 8%. For F_2^π , detector-related effects—such as the forward baryon reconstruction efficiency and t resolution—constitute the dominant sources of systematic uncertainty, contributing roughly 10%. In contrast, for F_2^K , these detector effects are mitigated by the presence of charged decay channels, reducing their impact to approximately 5%.

At the results level, EicC measurements of F_2^π exhibit a pronounced advantage in the medium-to-large x_π region and can provide complementary constraints to existing Drell–Yan data, thereby further reducing the theoretical uncertainties associated with meson flux factors. In contrast, experimental information on the kaon structure function remains extremely limited; what is exciting is that EicC will provide a particularly valuable opportunity for systematic, high-precision measurements of F_2^K across a broad kinematic range. Leverag-

ing the efficient reconstruction of $\Lambda \rightarrow p\pi^-$ decays, superior resolution in momentum transfer can be achieved for the kaon measurement, enhancing the overall feasibility of measuring F_2^K .

Our study suggests that, even with the present detector performance assumptions, EicC will serve as an ideal facility for probing the internal structure of pions and kaons. The detector design is still under ongoing optimization. In particular, with more advanced detector technology, the energy resolution of ZDC is expected to reach approximately $35\%/\sqrt{E}$, which will further reduce the systematic uncertainties in the extraction of F_2^π . For kaon measurements, although the neutral decay channel of the Λ has a relatively small branching ratio, it is in principle feasible to reconstruct its decay topology using the forward detector system. At the current stage, however, the main limitation arises from the insufficient size of the ZDC, which leads to a low neutron acceptance, as illustrated in Fig. 6(a). To address this issue, one possible improvement is to install an additional hadronic calorimeter downstream of the EDT-ECal system to enhance the acceptance for neutral particles. Such an upgrade would require coordinated design with the beamline. In addition, given the different PID requirements, the neutral decay channel would help constrain the systematic uncertainties in F_2^K due to PID, thereby enhancing the robustness of the meson-structure studies at EicC.

In summary, EicC will provide essential and high-precision experimental input for understanding the quark structure of light mesons under strong interactions, offering a valuable testing ground for non-perturbative QCD.

VI. ACKNOWLEDGMENTS

We would like to express our heartfelt gratitude to Craig D. Roberts, Tanja Horn, Garth M. Huber, Jixie Zhang, Richard Trotta and Avnish Singh for their invaluable theoretical guidance and technical support throughout this work. We also sincerely thank Jianing Dong for ensuring the excellent performance and reliability of the computer facility at Shandong University, which made our computations possible.

This work is supported by the National Natural Science Foundation of China under Grant Nos. 12305144 and 12375139, the Shandong Province Natural Science Foundation under Grant Nos. 2023HWYQ-010 and ZR2022QA032, and the National Key Research and

- [1] Y. Nambu, Phys. Rev. **117**, 648 (1960).
- [2] J. Goldstone, Nuovo Cim. **19**, 154 (1961).
- [3] A. Deur, S. J. Brodsky, and G. F. de Teramond, Phys. Lett. B **757**, 275 (2016), arXiv:1601.06568 [hep-ph].
- [4] A. Deur, S. J. Brodsky, and G. F. de Teramond, Nucl. Phys. **90**, 1 (2016), arXiv:1604.08082 [hep-ph].
- [5] G. F. de Teramond, S. J. Brodsky, A. Deur, H. G. Dosch, and R. S. Sufian, EPJ Web Conf. **137**, 03023 (2017), arXiv:1611.03763 [hep-ph].
- [6] C. D. Roberts, D. G. Richards, T. Horn, and L. Chang, Prog. Part. Nucl. Phys. **120**, 103883 (2021), arXiv:2102.01765 [hep-ph].
- [7] X. Gao, L. Jin, C. Kallidonis, N. Karthik, S. Mukherjee, P. Petreczky, C. Shugert, S. Syritsyn, and Y. Zhao, Phys. Rev. D **102**, 094513 (2020), arXiv:2007.06590 [hep-lat].
- [8] X. Gao, N. Karthik, S. Mukherjee, P. Petreczky, S. Syritsyn, and Y. Zhao, Phys. Rev. D **104**, 114515 (2021), arXiv:2102.06047 [hep-lat].
- [9] H.-T. Ding, X. Gao, A. D. Hanlon, S. Mukherjee, P. Petreczky, Q. Shi, S. Syritsyn, R. Zhang, and Y. Zhao, Phys. Rev. Lett. **133**, 181902 (2024), arXiv:2404.04412 [hep-lat].
- [10] J.-W. Chen, H.-W. Lin, and J.-H. Zhang, Nucl. Phys. B **952**, 114940 (2020), arXiv:1904.12376 [hep-lat].
- [11] H.-W. Lin, J.-W. Chen, Z. Fan, J.-H. Zhang, and R. Zhang, Phys. Rev. D **103**, 014516 (2021), arXiv:2003.14128 [hep-lat].
- [12] C. D. Roberts and A. G. Williams, Prog. Part. Nucl. Phys. **33**, 477 (1994), arXiv:hep-ph/9403224.
- [13] P. Maris, C. D. Roberts, and P. C. Tandy, Phys. Lett. B **420**, 267 (1998), arXiv:nucl-th/9707003.
- [14] L. Chang, I. C. Cloet, J. J. Cobos-Martinez, C. D. Roberts, S. M. Schmidt, and P. C. Tandy, Phys. Rev. Lett. **110**, 132001 (2013), arXiv:1301.0324 [nucl-th].
- [15] C. Shi, C. Mezrag, and H.-s. Zong, Phys. Rev. D **98**, 054029 (2018), arXiv:1806.10232 [nucl-th].
- [16] K. D. Bednar, I. C. Cloët, and P. C. Tandy, Phys. Rev. Lett. **124**, 042002 (2020),

- arXiv:1811.12310 [nucl-th].
- [17] R. Machleidt and D. R. Entem, Phys. Rept. **503**, 1 (2011), arXiv:1105.2919 [nucl-th].
 - [18] S. Weinberg, Nucl. Phys. B **363**, 3 (1991).
 - [19] P. T. P. Hutaauruk, W. Bentz, I. C. Cloët, and A. W. Thomas, Phys. Rev. C **97**, 055210 (2018), arXiv:1802.05511 [nucl-th].
 - [20] K. Park *et al.* (CLAS), Eur. Phys. J. A **49**, 16 (2013), arXiv:1206.2326 [nucl-ex].
 - [21] A. Airapetian *et al.* (HERMES), Phys. Lett. B **659**, 486 (2008), arXiv:0707.0222 [hep-ex].
 - [22] E. B. Dally *et al.*, Phys. Rev. D **24**, 1718 (1981).
 - [23] E. B. Dally *et al.*, Phys. Rev. Lett. **48**, 375 (1982).
 - [24] S. R. Amendolia *et al.*, Phys. Lett. B **146**, 116 (1984).
 - [25] S. R. Amendolia *et al.* (NA7), Nucl. Phys. B **277**, 168 (1986).
 - [26] L. Favart, M. Guidal, T. Horn, and P. Kroll, Eur. Phys. J. A **52**, 158 (2016), arXiv:1511.04535 [hep-ph].
 - [27] C. N. Brown, C. R. Canizares, W. E. Cooper, A. M. Eisner, G. J. Feldmann, C. A. Lichtenstein, L. Litt, W. Loceretz, V. B. Montana, and F. M. Pipkin, Phys. Rev. D **8**, 92 (1973).
 - [28] C. L. Arnold, B. P. Roe, and D. Sinclair, Phys. Rev. D **9**, 1221 (1974).
 - [29] C. J. Bebek *et al.*, Phys. Rev. D **17**, 1693 (1978).
 - [30] H. Ackermann, T. Azemoon, W. Gabriel, H. D. Mertiens, H. D. Reich, G. Specht, F. Janata, and D. Schmidt, Nucl. Phys. B **137**, 294 (1978).
 - [31] P. Brauel, T. Canzler, D. Cords, R. Felst, G. Grindhammer, M. Helm, W. D. Kollmann, H. Krehbiel, and M. Schadlich, Z. Phys. C **3**, 101 (1979).
 - [32] V. Tadevosyan *et al.* (Jefferson Lab F(pi)), Phys. Rev. C **75**, 055205 (2007), arXiv:nucl-ex/0607007.
 - [33] T. Horn *et al.* (Jefferson Lab F(pi)-2), Phys. Rev. Lett. **97**, 192001 (2006), arXiv:nucl-ex/0607005.
 - [34] M. Carmignotto *et al.*, Phys. Rev. C **97**, 025204 (2018), arXiv:1801.01536 [nucl-ex].
 - [35] A. Accardi *et al.*, Eur. Phys. J. A **60**, 173 (2024), arXiv:2306.09360 [nucl-ex].
 - [36] T. Horn *et al.*, Phys. Rev. C **78**, 058201 (2008), arXiv:0707.1794 [nucl-ex].
 - [37] G. M. Huber *et al.* (Jefferson Lab), Phys. Rev. C **78**, 045203 (2008), arXiv:0809.3052 [nucl-ex].
 - [38] Measurement of Tagged Deep Inelastic Scattering (TDIS), https://www.jlab.org/exp_prog/proposals/14/PR12-14-010.pdf (), accessed: 2021-09-16.

- [39] Measurement of Kaon Structure Function through Tagged Deep Inelastic Scattering (TDIS), https://www.jlab.org/exp_prog/proposals/17/C12-15-006A.pdf (), accessed: 2021-09-16.
- [40] D. R. DeBoer *et al.*, Publ. Astron. Soc. Pac. **129**, 045001 (2017), arXiv:1606.07473 [astro-ph.IM].
- [41] F. D. Aaron *et al.* (H1), Eur. Phys. J. C **68**, 381 (2010), arXiv:1001.0532 [hep-ex].
- [42] S. Chekanov *et al.* (ZEUS), Nucl. Phys. B **637**, 3 (2002), arXiv:hep-ex/0205076.
- [43] C. Quintans (AMBER), Few Body Syst. **63**, 72 (2022).
- [44] B. Adams *et al.*, Letter of Intent: A New QCD facility at the M2 beam line of the CERN SPS (COMPASS++/AMBER) (2018), cERN-SPSC-2019-003, SPSC-I-250, arXiv:1808.00848 [hep-ex].
- [45] A. C. Aguilar *et al.*, Eur. Phys. J. A **55**, 190 (2019), arXiv:1907.08218 [nucl-ex].
- [46] J. Arrington *et al.*, J. Phys. G **48**, 075106 (2021), arXiv:2102.11788 [nucl-ex].
- [47] R. Abdul Khalek *et al.*, Nucl. Phys. A **1026**, 122447 (2022), arXiv:2103.05419 [physics.ins-det].
- [48] M. Ding, C. D. Roberts, and S. M. Schmidt, Particles **6**, 57 (2023), arXiv:2211.07763 [hep-ph].
- [49] E. Ruiz Arriola and P. Sanchez-Puertas, Phys. Rev. D **110**, 054003 (2024), arXiv:2403.07121 [hep-ph].
- [50] J. D. Sullivan, Phys. Rev. D **5**, 1732 (1972).
- [51] C. Adloff *et al.* (H1), Eur. Phys. J. C **6**, 587 (1999), arXiv:hep-ex/9811013.
- [52] D. P. Anderle *et al.*, Front. Phys. (Beijing) **16**, 64701 (2021), arXiv:2102.09222 [nucl-ex].
- [53] H. Holtmann, G. Levman, N. N. Nikolaev, A. Szczurek, and J. Speth, Phys. Lett. B **338**, 393 (1995), arXiv:hep-ph/9602229.
- [54] J. R. McKenney, N. Sato, W. Melnitchouk, and C.-R. Ji, Phys. Rev. D **93**, 054011 (2016), arXiv:1512.04459 [hep-ph].
- [55] V. P. Goncalves, F. S. Navarra, and D. Spiering, Phys. Rev. D **93**, 054025 (2016), arXiv:1512.06594 [hep-ph].
- [56] G. Xie, C. Han, R. Wang, and X. Chen, Chin. Phys. C **46**, 064107 (2022), arXiv:2109.08483 [hep-ph].
- [57] R. Wang, G. Xie, W. Xiong, Y. Liang, and X. Chen, Few Body Syst. **64**, 28 (2023).
- [58] G. Xie, M. Li, C. Han, R. Wang, and X. Chen, Chin. Phys. C **45**, 053002 (2021), arXiv:2009.04956 [hep-ph].

- [59] M. Bishari, Phys. Lett. B **38**, 510 (1972).
- [60] H. Holtmann, G. Levman, N. N. Nikolaev, A. Szczurek, and J. Speth, Phys. Lett. B **338**, 363 (1994).
- [61] B. Kopeliovich, B. Povh, and I. Potashnikova, Z. Phys. C **73**, 125 (1996), arXiv:hep-ph/9601291.
- [62] R. G. E. Timmermans, T. A. Rijken, and J. J. de Swart, Phys. Rev. Lett. **67**, 1074 (1991).
- [63] C. Xu, C. Lei, C. Ningbo, *et al.*, NUCLEAR TECHNIQUES **43**, 1 (2020).
- [64] X. Chen, PoS **DIS2018**, 170 (2018), arXiv:1809.00448 [nucl-ex].
- [65] S. Zhu, D. Zheng, L. Xia, and Y. Zhang, Phys. Rev. D **111**, 076024 (2025), arXiv:2409.00653 [hep-ph].
- [66] D. P. Anderle, A. Guo, F. Hekhorn, Y. Liang, Y. Ma, L. Xia, H. Xing, and Y. Zhao, Phys. Rev. D **109**, 034021 (2024), arXiv:2307.16135 [nucl-ex].
- [67] S. Agostinelli *et al.* (GEANT4), Nucl. Instrum. Meth. A **506**, 250 (2003).
- [68] rong-wang impcas, <https://github.com/rong-wang-impcas/tagged-neutron-DIS> (), accessed: 2023-08-24.
- [69] rong-wang impcas, <https://github.com/rong-wang-impcas/tagged-Lambda-DIS> (), accessed: 2023-08-24.
- [70] R. Brun and F. Rademakers, Nucl. Instrum. Meth. A **389**, 81 (1997).
- [71] P. C. Barry, N. Sato, W. Melnitchouk, and C.-R. Ji, Phys. Rev. Lett. **121**, 152001 (2018), arXiv:1804.01965 [hep-ph].
- [72] C. Han, H. Xing, X. Wang, Q. Fu, R. Wang, and X. Chen, Phys. Lett. B **800**, 135066 (2020), arXiv:1809.01549 [hep-ph].
- [73] lukeronger/piIMParton, <https://github.com/lukeronger/piIMParton>, accessed: 2020-09-01.
- [74] P. C. Barry, C.-R. Ji, W. Melnitchouk, N. Sato, and F. Steffens (JAM), First simultaneous global QCD analysis of kaon and pion parton distributions with lattice QCD constraints (2025), arXiv:2510.11979 [hep-ph].
- [75] C. Bourrely, F. Buccella, W.-C. Chang, and J.-C. Peng, Phys. Lett. B **848**, 138395 (2024), arXiv:2305.18117 [hep-ph].
- [76] W.-C. Chang, J.-C. Peng, S. Platchkov, and T. Sawada, Phys. Lett. B **855**, 138820 (2024), arXiv:2402.02860 [hep-ph].

- [77] C. Han, G. Xie, R. Wang, and X. Chen, Eur. Phys. J. C **81**, 302 (2021), arXiv:2010.14284 [hep-ph].
- [78] J. Badier *et al.* (Saclay-CERN-College de France-Ecole Poly-Orsay), Phys. Lett. B **93**, 354 (1980).
- [79] S. Navas *et al.* (Particle Data Group), Phys. Rev. D **110**, 030001 (2024).
- [80] C. Bierlich *et al.*, SciPost Phys. Codeb. **2022**, 8 (2022), arXiv:2203.11601 [hep-ph].
- [81] T. M. Aliev and M. Savci, Phys. Rev. C **61**, 045201 (2000), arXiv:hep-ph/9902466.
- [82] R. A. Adelseck and B. Saghai, Phys. Rev. C **42**, 108 (1990).
- [83] R. A. Williams, C. R. Ji, and S. R. Cotanch, Phys. Rev. C **43**, 452 (1991).
- [84] R. A. Williams, C. R. Ji, and S. R. Cotanch, Phys. Rev. C **46**, 1617 (1992).
- [85] T. Mart, C. Bennhold, and C. E. Hyde, Phys. Rev. C **51**, R1074 (1995), arXiv:nucl-th/9502016.
- [86] J. C. David, C. Fayard, G. H. Lamot, and B. Saghai, Phys. Rev. C **53**, 2613 (1996).
- [87] I. J. General and S. R. Cotanch, Phys. Rev. C **69**, 035202 (2004), arXiv:nucl-th/0311039.
- [88] M. Guidal, J. M. Laget, and M. Vanderhaeghen, Nucl. Phys. A **627**, 645 (1997).
- [89] F. X. Lee, T. Mart, C. Bennhold, and L. E. Wright, Nucl. Phys. A **695**, 237 (2001), arXiv:nucl-th/9907119.
- [90] A. D. Martin, Nucl. Phys. B **179**, 33 (1981).
- [91] C. Gobbi, D. O. Riska, and N. N. Scoccola, Nucl. Phys. A **544**, 671 (1992).
- [92] S. Choe, M. K. Cheoun, and S. H. Lee, Phys. Rev. C **53**, 1363 (1996), arXiv:nucl-th/9508037.
- [93] W.-T. Chiang, F. Tabakin, T. S. H. Lee, and B. Saghai, Phys. Lett. B **517**, 101 (2001), arXiv:nucl-th/0104052.
- [94] J. Badier *et al.* (NA3), Z. Phys. C **18**, 281 (1983).
- [95] D. Adikaram *et al.*, *Measurement of Tagged Deep Inelastic Scattering (TDIS)*, Experiment Proposal PR12-15-006 (Thomas Jefferson National Accelerator Facility, 2015).
- [96] M. B. Hecht, C. D. Roberts, and S. M. Schmidt, Phys. Rev. C **63**, 025213 (2001), arXiv:nucl-th/0008049.
- [97] Z.-F. Cui, M. Ding, F. Gao, K. Raya, D. Binosi, L. Chang, C. D. Roberts, J. Rodríguez-Quintero, and S. M. Schmidt, Eur. Phys. J. C **80**, 1064 (2020).
- [98] B. Betev *et al.* (NA10), Z. Phys. C **28**, 9 (1985).